



22 **Abstract**

23

24 The detection of meteorological, chemical, or other signals in modeled or observed air quality
25 data – such as an estimate of a temporal trend in surface ozone data, or an estimate of the mean
26 ozone of a particular region during a particular season – is a critical component of modern
27 atmospheric chemistry. However, the magnitude of a surface air quality signal is generally small
28 compared to the magnitude of the underlying chemical and meteorological variabilities that exist
29 both in space and in time. This can present difficulties for both policy-makers and researchers as
30 they attempt to identify the influence or 'signal' of climate trends (e.g. any pauses in warming
31 trends), the impact of enacted emission reductions policies (e.g. United States NO_x State
32 Implementation Plans), or an estimate of the mean state of highly variable data (e.g. summertime
33 ozone over the Northeastern United States). Here we examine the scale-dependence of the
34 variability of simulated and observed surface ozone data within the United States and the
35 likelihood that a particular choice of temporal or spatial averaging scales produce a misleading
36 estimate of a particular ozone signal. Our main objective is to develop strategies that reduce the
37 likelihood of overconfidence in simulated ozone estimates. We find that while increasing the
38 extent of both temporal and spatial averaging can enhance signal detection capabilities by
39 reducing the 'noise' from variability, a strategic combination of particular temporal and spatial
40 averaging scales can maximize signal detection capabilities over much of the Continental US.
41 We recommend temporal averaging of at least 10 - 15 years combined with regional spatial
42 averaging over several hundred kilometer spatial scales. These results are consistent between
43 simulated and observed data, and within a single model with different sets of parameters. The
44 strategies selected in this study are not limited to surface ozone data, and could potentially
45 maximize signal detection capabilities within a broad array of climate and chemical observations
46 or model output.

47



48 **Copyright Statement**

- 49 • Authors retain the copyright of the article. Regarding copyright transfers please see
50 below.
- 51 • Authors grant Copernicus Publications an irrevocable non-exclusive license to publish
52 the article electronically and in print format and to identify itself as the original publisher.
- 53 • Authors grant Copernicus Publications commercial rights to produce hardcopy volumes
54 of the journal for sale to libraries and individuals.
- 55 • Authors grant any third party the right to use the article freely as long as its original
56 authors and citation details are identified.
- 57 • The article is distributed under the Creative Commons Attribution 4.0 License. Unless
58 otherwise stated, associated published material is distributed under the same license.
59



60 **1 Introduction**

61 The capability to detect air quality signals – be they meteorological, chemical, or of some
62 other type – is a fundamental component of modern climate science and atmospheric chemistry.
63 The debate over the existence or length of a global warming hiatus (Lewandowski et al., 2015;
64 Roberts et al., 2015; Medhaug et al., 2017) and research examining the time of emergence of
65 climatological (Hawkins and Sutton, 2012; Elía et al., 2013; Schurer et al., 2013), meteorological
66 (Giorgi and Bi, 2009; King et al., 2015), chemical (Barnes et al., 2016; Garcia-Menendez et al.,
67 2017), and other sectoral signals (e.g. Monier et al., 2016) embody an accumulation of
68 techniques and strategies for filtering noise (due to natural variability) and maximizing the
69 capability to detect statistically significant signals and trends in noisy data. It is well established
70 that temporal averaging (e.g. Lewandowski et al., 2015) and spatial averaging (e.g. Frost et al.,
71 2006; Hawkins and Sutton, 2012; Barnes et al., 2016) can enhance signal detection capabilities
72 in atmospheric data. Here we extend this research by quantifying the impact of both spatial and
73 temporal averaging – individually and in combination – of surface ozone on the magnitude of the
74 calculated variability, which is largely driven by the influence of meteorological variability on
75 the atmospheric chemistry (e.g. Jacob and Winner, 2009). We offer recommendations for
76 strategically averaging in space and time to maximize signal detection capabilities. In particular,
77 we examine estimates of mean ozone and of the ozone variability that results from meteorology,
78 although our approach can be generalized to other air quality applications.

79 For observed ozone data, strategies for reducing spatial and temporal noise are limited: a
80 longer time series is needed, more observations need to be made, or the spatial region over which
81 the ozone observations are being averaged over needs to be enlarged. For surface ozone
82 estimates using models, however, there exist a variety of strategies for reducing the noise (due to
83 chemical and meteorological variability) relative to the strength of the signal, although they
84 cluster into three main types. The first strategy is to average or combine multiple runs of
85 structurally different models under the assumption that errors, biases, and uncertainties within
86 the individual models are reduced and the multi-model or multi-dataset mean is a best estimate
87 of the actual, aggregated ozone field. This is most notably done with multi-model ensembles
88 within the ACCMIP framework (Lamarque et al., 2013; Young et al., 2013; Stevenson et al.,
89 2013), and this approach tends to assume that all members in the ensemble are independent and
90 equally skillful. This assumption, however, may result in a loss of some valuable information



91 (Knutti, 2010). Another form of this strategy is to run multiple model runs within a single model,
92 but under different initial conditions or sets of parametric assumptions (e.g. Deser et al, 2010;
93 Monier et al., 2013, 2015; Kay et al., 2015; Garcia-Menendez et al., 2015, 2017). This approach
94 cannot address structural uncertainties between models, but is capable of identifying parametric
95 uncertainties within a single model.

96 The second strategy to reduce ozone variability is to expand the temporal averaging window,
97 which can influence the interpretation of the determined ozone value (e.g. Brown-Steiner et al.,
98 2015). The Environmental Protection Agency (EPA) National Ambient Air Quality Standard
99 (NAAQS) for ozone (US EPA, 2015) explicitly takes this into account, both in the length of the
100 averaging period (daily maximum 8-hour average) and the selection criteria for the standard
101 (fourth-highest over the previous 3 years). The calculated ozone variability can be further
102 reduced by utilizing even longer averaging periods, such as monthly (e.g. Rasmussen et al.,
103 2012), seasonal (e.g. Fiore et al., 2014; Barnes et al., 2016), annual, or decadal mean values (e.g.
104 Garcia-Menendez et al., 2017). This strategy is analogous to the averaging of meteorological
105 data to derive a climate signal, and just as Lewandowsky et al. (2015) recommend averaging 17
106 or more years in order to achieve climatological estimates of temperature trends, there is a
107 growing body of literature recommending averaging short time scale chemical variability (what
108 could be called chemical weather, see Lawrence, 2005) for 15 or more years (e.g. Garcia-
109 Menendez et al, 2017) in order to achieve an estimate of the what could be called the chemical
110 climate (see Möller, 2010).

111 The third strategy to reduce ozone variability is to average surface ozone values over larger
112 spatial regions, and while there is a significant body of literature discussing the capability and
113 interpretation of coarse resolution model representations of the sub-grid scale heterogeneity
114 (Pyle and Zavody, 1990; Searle et al., 1998, Wild et al., 2006), there are few that strategically
115 expand the spatial scale over which averaging is applied in order to maximize signal detection
116 capabilities. This strategy has been applied in other fields of the atmospheric sciences as well as
117 for general gridded datasets (e.g. Pogson and Smith, 2015), and spatial averaging has been
118 suggested as a means of reducing temperature variability and smoothing biases at the smallest
119 spatial scales within a single model run (Räisänen and Ylhäsi, 2011). This “scale problem” has
120 also been noted as an important consideration when analyzing aerosol indirect effects



121 (McComiskey and Feingold, 2012) and for the detection and attribution of extreme weather
122 events (Angélil et al., 2017).

123 Our objective in this study is to provide a framework for selecting spatial and temporal
124 averaging scales that limits the likelihood of over-confidence in an estimate of surface ozone that
125 arises from meteorological variability. This type of framework can be useful from two different
126 research perspectives. The first research perspective has a priori an ozone estimate (either
127 observed or modeled) at a certain spatial and temporal scale (e.g. a 3-year simulation of surface
128 ozone over the Northeastern US) and wants to quantify the likelihood that this estimate is
129 representative of the long-term ozone behavior (rather than overly sensitive to meteorological
130 variability of that particular 3-year period). Since ozone is strongly influenced by natural
131 fluctuations in meteorology (Jacob and Winner, 2009; Jhun et al., 2015) and since extremes in
132 surface ozone and temperature tend to co-occur (Schnell and Prather, 2017), atypically hot or
133 cold periods can strongly influence ozone behavior over short time scales.

134 The second research perspective is to identify an ozone signal of a certain magnitude (or
135 threshold) and needs to decide what spatial and temporal averaging scales are needed to best
136 identify that signal. The ozone signal could be large (e.g. determining the effectiveness or
137 compliance with a 5 ppbv incremental reduction of the EPA NAAQS for ozone (US EPA, 2015))
138 or small (e.g. identifying annual ozone trends within the US, which Cooper et al. (2012) show
139 can be on the order of 0.10 – 0.45 ppbv), and can be highly sensitivity to spatial and temporal
140 heterogeneity and meteorological variability. Barnes et al. (2016) found that surface ozone trends
141 over 20-year periods can vary by ± 2 ppbv due solely to climate variability, while interannual
142 variability can be on the order of ± 15 ppbv (Fiore et al., 2003; Tilmes et al., 2012; Line et al.,
143 2014) and day-to-day variability can be even larger, extending regularly from near-background
144 levels of 40 – 50 ppbv up to 100 ppbv during the summertime (Fiore et al., 2014).

145 In this study, we quantify the impact of both temporal and spatial averaging on the calculated
146 ozone variability – due solely to meteorological variability – in order to maximize the capability
147 to detect trends. We use simulated ozone (with the Community Atmosphere Model with
148 Chemistry, CAM-chem) and observational data (with the EPA’s Clean Air Status and Trends
149 Network, CASTNET) within the United States in order to answer the following four questions:
150 (1) Within a given dataset (model or observations), with both spatial and temporal coverage,
151 what is the magnitude of the ozone variability due to meteorology at the smallest scale, and how



152 does spatial and temporal averaging reduce this variability? (2) Are there combinations of
153 temporal and spatial averaging scales that maximize the signal detection capability for surface
154 ozone data? (3) How sensitive are the above strategies to different configurations (i.e. emissions,
155 meteorology, and climate) of the CAM-chem modeling framework? And (4) How could they be
156 applied to other datasets (chemical, meteorological, or climatological)? We limit our focus to
157 spatial scales within the United States as it has high spatial and temporal variability and
158 numerous observations, and since averaging over larger regions (e.g. the Northern Hemisphere,
159 or the globe) would produce a smaller calculated variability.

160 In Section 2, we describe the CAM-chem model and our simulations, as well as the
161 CASTNET observational database and the regional definitions used throughout this paper. In
162 Section 3 we quantify the temporal and spatial variability of surface ozone, show how temporal
163 and spatial averaging reduces the calculated ozone variability, and demonstrate the spatial
164 heterogeneity of the calculated ozone variability. In Section 4, we discuss the potential strategies
165 that could be used to maximize ozone trend detection due to meteorological variability, explore
166 uncertainties, and make recommendations for future research.

167

168 **2 Methods**

169

170 We examine both present-day (one simulation and one observed dataset) and future (two
171 simulations) surface ozone in this study. For present-day analysis, we simulate surface ozone
172 using CAM-chem, a component of the Community Earth System Model (CESM) and available
173 observations within the US from the EPA CASTNET database. For future analysis, and in order
174 to examine the potential for patterns of variability to change in the future, we utilize two existing
175 simulations of CAM-chem conducted by Garcia-Menendez et al. (2017). Much of this analysis is
176 conducted using the R language (R-Project, www.r-project.org). Here we summarize each of the
177 three datasets and our approach to our analysis in Section 3.

178

179 **2.1 CAM-chem**

180 The present-day simulation (MOZ_2000) was conducted using CAM-chem model
181 version 1.2.2, with the CAM4 atmospheric component (Tilmes et al., 2015; 2016). The model
182 has been used extensively for a wide range of atmospheric chemistry research and included in
183 the Atmospheric Chemistry and Climate Model Intercomparison Project (ACCMIP, Lamarque et



184 al., 2012; Young et al., 2012 and references therein). We conduct our simulations using the
185 MOZART-4 chemical mechanism (Emmons et al., 2010) with offline forced meteorology from
186 the Modern-Era Retrospective analysis for Research and Applications (MERRA) reanalysis
187 product (Rienecker et al., 2011) for 26 meteorological years (1990 – 2015). This simulation has
188 56 vertical levels – adopted from MERRA meteorology – and 96 latitudinal and 144 longitudinal
189 grid cells. We aim to isolate the variability to the meteorologically-driven impact on atmospheric
190 chemistry so we repeat year-2000 anthropogenic emissions from the ACCMIP (Atmospheric
191 Chemistry and Climate Model Intercomparison Project) inventory (Lamarque et al., 2012) and
192 all non-biogenic emissions for all meteorological years, and include specified long-lived
193 stratospheric species (O_3 , NO_x , HNO_3 , N_2O , N_2O_5) as in MOZART-4 (Emmons et al., 2010), an
194 online biogenic emissions model MEGAN (Guenther et al., 2012), and forced sea ice and sea
195 surface temperatures to year 2000 historical conditions. Like many state-of-the-art chemical
196 tracer models, the CAM-chem exhibits some biases, most notably for our purposes a high bias in
197 simulated surface ozone in the Eastern US (e.g. Lamarque et al., 2012; Brown-Steiner et al.,
198 2015; Travis et al., 2016; Barnes et al., 2016). Recent efforts have been successful in partially
199 reducing these biases (e.g. Sun et al., 2017).

200 We also include two reference simulations of the future, MOZ_2050 and MOZ_2100
201 (simulating the meteorological years 2035 – 2065 and 2085 – 2115, respectively) using the
202 CESM CAM-chem simulations described in detail by Garcia-Menendez et al. (2017) with one
203 set of initial condition data, and a climate sensitivity of 3.0 °C. Compared to the present-day
204 simulations, these future simulations have several parametric differences: the model version is
205 1.1.2, the atmospheric component is CAM3, the emissions (which are held constant at year-2000
206 levels) are from the Precursors of Ozone and their Effects in the Troposphere database (see
207 Garcia-Menendez et al., 2017), and the meteorology is derived from a linkage between the
208 Massachusetts Institute of Technology Integrated Global System Model (MIT IGSM) and the
209 CESM CAM model (Monier et al., 2013), and as such has 26 vertical levels. For a full
210 description of these simulations, see Garcia-Menendez et al. (2017).

211

212 2.2 CASTNET

213 The observational database comes from the EPA Clean Air Status and Trends Network
214 (CASTNET), which has more than 90 surface observational sites within the United States and



215 has been collecting hourly surface meteorological and chemical data since 1990 (US EPA, 2016
216 and <https://www.epa.gov/castnet>). We collected data from all sites that reported complete ozone
217 data from each year and removed data that was marked invalid within the downloaded EPA files.
218 The number of sites that matched these criteria varied from year to year, but generally we have
219 between 55 and 94 sites throughout the 1991 – 2014 period. The CASTNET observational
220 network is located primarily in rural sites, and thus is considered to be a reasonable comparison
221 to coarse grid cell model output. Since a notable trend in observed ozone data exists, especially
222 in the Northeastern US (Frost et al., 2006), and since the simulations have no change in
223 anthropogenic emissions, and thus no ozone trend, we detrended the CASTNET data for each of
224 the four averaging regions (described below) using a simple linear regression.

225

226 **2.3 Telescoping Regional Definitions**

227 In order to isolate the impact of the size of the spatial scale over which ozone data is
228 averaged, we analyze ozone data at different spatial scales. The largest region considered is the
229 entire Continental US, while the smallest regions considered are at the individual grid cell level
230 of the CESM CAM-chem model (1.9°x2.5° latitude/longitude). We focus on the US since there
231 are CASTNET observations that provide adequate coverage in both space and time, and since the
232 US has significant temporal and spatial variability. Data and statistics for the other regions (i.e.
233 the Midwestern and Southeastern US) are included in the Supplemental Material, but do not alter
234 the conclusions we draw from the Northeastern US. For CESM CAM-chem data, we averaged
235 all grid cells within each region, while for the CASTNET data we first average sites within each
236 corresponding CESM CAM-chem grid cell, and then averaged these data together. These
237 telescoping regions are shown in Figure 1.

238

239 **3 Results**

240 Here we examine the spatial and temporal behavior of MOZ_2000, MOZ_2050, and
241 MOZ_2100 and compare MOZ_2000 to present-day CASTNET observations. We introduce the
242 moving temporal averaging windows, explore possible thresholds of acceptable error or signal
243 strength, and examine the influence of expanding spatial averaging regions. Finally, we combine
244 these temporal and spatial averaging techniques into a single framework.

245



246 **3.1 Spatial and Temporal Comparisons**

247 Figure 2 plots the averaged spatial distribution of the daily maximum 8-hour ozone
248 average (DM8H O₃) for summertime (JJA) days for 1990-2015 for the present-day MOZART
249 simulation, MOZ_2000 (Figure 2a) and for the year 2000 for CASTNET data (Figure 2b). The
250 well-known high ozone bias in the Eastern US (e.g. Lamarque et al., 2012; Travis et al., 2016;
251 Barnes et al., 2016) is apparent, but otherwise the spatial variability over the entire Continental
252 US is well captured. While we do examine the magnitude of surface ozone in this paper, most of
253 our analysis is focused on the variability around the mean value (the anomaly), and as we show
254 below, the CASTNET observations and CESM results are largely consistent in their
255 representation of ozone variability. The standard deviation of DM8H O₃ is large over the Eastern
256 US and the Pacific Coast, with peak values of ± 25 ppbv over the highly populated Atlantic
257 Coast (Figure 2c). The variability (defined as the standard deviation divided by the mean,
258 expressed as a percentage) is lowest over the Western US (~ 15%), only slightly higher over the
259 Eastern US (up to 25%), and highest (up to 50%) over the coastal regions (Figure 2d). The future
260 simulations, MOZ_2050 and MOZ_2100 (Figure 2e and 2f, respectively), although run with
261 different parametric settings than MOZ_2000 (see Section 2), simulate a similar spatial
262 distribution of surface ozone, although under the warmer simulated climate of 2050 and 2100.
263 These future simulations have a similar spatial pattern to the present-day simulation (Figure 2a),
264 with high ozone levels in the Eastern US that increases from 2050 to 2100 (see Garcia-Menendez
265 et al. (2017) for more details).

266 Figure 3 compares boxplots over the four telescoping regions (Figure 1) for MOZ_2000,
267 the CASTNET data, the detrended CASTNET data, and for the single year 2000 for the
268 CASTNET data (Figures 3a-d), and Table 1 summarizes relevant statistics. In order to compare
269 CASTNET ozone to the simulated ozone, which do not have a trend over time, we detrend the
270 CASTNET data in order to remove the impact of any temporal trends (e.g. NO_x emissions
271 reductions) on ozone. The Northeastern US ozone bias is apparent at the smaller spatial scales
272 (Figures 3c,d) and is less apparent when averaging over larger regions (Figures 3a,b). Figure 3e
273 compares the year-to-year boxplots of the JJA DM8H O₃ for the MOZ_2000 and the detrended
274 CASTNET data, and demonstrates the variability both in the median and spread of the ozone
275 values in both the modeled and simulated data. While the MOZ_2000 ozone is generally higher
276 than the CASTNET data, there are years in which the CASTNET data has higher ozone



277 extremes. The red box plot in Figure 3e, which corresponds to the red box plot in Figure 3b,
278 indicates that the year 2000 was an anomalously low year for observed ozone, although not the
279 lowest.

280 While all the CESM CAM-chem simulations have high ozone biases in the Northeastern
281 US (Figures 2 and 3, Table 1), their capability to simulate ozone variability is consistent with the
282 available observations (for present day) and for expectations of ozone variability changes in the
283 future (for MOZ_2050 and MOZ_2100). Here we examine the variability defined as the standard
284 deviation divided by the mean (expressed as a percent), instead of the standard deviation alone,
285 in order to account for the model biases in the magnitude of the simulated ozone. It is clear that
286 variability increases when the size of the averaging region decreases, a fact that is well noted in
287 the literature, as in Hawkins and Sutton (2012) for climate variables and Barnes et al. (2016) for
288 ozone. As can be seen in in Table 1, the CASTNET variability increases as the spatial scale
289 decreases (10%, 13%, 16%, and 20% for our telescoping regions), and MOZ_2000 largely
290 captures this trend (5%, 10%, 15%, and 15%). This increase in ozone variability with decreasing
291 spatial scale is maintained in the future simulations (6%, 10%, 16%, and 21% for MOZ_2050
292 and 7%, 12%, 17%, and 20% for MOZ_2100). Table S1 contains statistics for the other
293 telescoping regions.

294

295

296 **3.2 Variability, Averaging Windows, and Thresholds**

297 As we aim to quantify the potential tradeoffs that result from a particular choice of
298 temporal and spatial scales on the assessment of ozone variability within the US, we represent
299 the spatial scale by applying the telescoping regions (see Figure 1) and we represent the temporal
300 scale through the use of moving averaging windows that range from 1 day up to the full 26 years
301 for the CESM data (1990-2015), the full 24 years for the detrended CASTNET data (1991 –
302 2014), and the 30 years available from the future scenarios of Garcia-Menendez et al. (2017).
303 Each averaging window, therefore, can be considered to be a “sample” of possible realizations of
304 meteorology. For instance, a selection of an averaging window of 1 year has 26 possible slices
305 within the 1990 – 2015 MOZ_2000 data, while a selection of an averaging window of 10 years
306 has 17 possible slices within the CESM data ($N = \# \text{ years} - \text{length of window} + 1$). In this study,
307 we consider all realizations to be equally likely and compare them to each other and to the long-
308 term trend. However, if we were only able to simulate 5 years, we would not be able to compare



309 to the long-term trend, and so be unable to completely quantify the likelihood of error in the
310 context of the long-term behavior. We frame much of the following analysis from the
311 perspective of limited simulation length in order to approximate the question that decision-
312 makers and modelers face when constrained by limited computational capabilities or available
313 data: what's the likelihood that a particular estimate (of both the mean and the variability) is not
314 a true representation of the true mean and variability, but rather a product of the particular choice
315 of spatial and temporal scale?

316 Figure 4 presents this likelihood by plotting all possible estimates of DM8H O₃ (as
317 anomalies from the long-term mean) over all possible selections of averaging window (from 1
318 day up to the complete time series) for our telescoping regions. The semi-cyclical and highly
319 auto-correlated nature of surface ozone is apparent at all spatial scales, with alternating cycles of
320 anomalously high and low ozone. The temporal impact of anomalous ozone events is indicated
321 by the vertical and right-leaning diagonal striations, which show that anomalous ozone events
322 can impact estimates of ozone values within averaging windows up to 15 or 20 years. Figure 4
323 demonstrates how small-scale anomalously high or low ozone values (that come only from
324 meteorological variability) can impact temporal averages of 5, 10, or even 20 years. For instance,
325 a selected 5-year averaging window within the MOZ_2000 simulation averaged over the
326 Northeastern US could be 2.5 ppbv higher or lower than the 25-year mean value of 74 ppbv, a
327 difference of 7%. Horizontal lines in Figure 4 mark the length of averaging windows that are
328 needed to ensure that ozone variability does not exceed a given threshold (5, 1, and 0.5 ppbv for
329 solid, dashed, and dotted lines respectively). This difference is larger within smaller regions and
330 at the shorter selections of the averaging window. While the high and low ozone anomalies differ
331 in time between CASTNET, MOZ_2000, MOZ_2050, and MOZ_2100 in Figure 4, the impact of
332 spatial and temporal averaging is consistent.

333 We also quantify this variability in Supplemental Figures S1 and S2, which plots the
334 likelihood (as a percentage) that a particular selection of spatial (rows) and temporal (x-axis)
335 scale estimates ozone values that exceed a particular threshold (colored lines) away from the true
336 mean value. For instance, if we are interested in characterizing ozone behavior (e.g. estimating a
337 trend, or the mean value) in the Northeastern US, but were limited to a 5-year simulation, there is
338 more than a 50% likelihood that the simulated ozone is 1 ppbv away from the 26-year mean, and
339 an 80% likelihood that the discrepancy is greater than 0.5 ppbv. However, these data indicate



340 that there is a virtual certainty that the estimate will be within 2.5 ppbv of the true mean value.
341 We should note that, at the grid-cell level and within a 10-year period, the surface ozone
342 variability can exceed 1 ppbv but is unlikely to exceed 2.5 ppbv (Figure 4), and that a 20-year
343 trend is very likely to be able to identify significant ozone signals among the impact of
344 meteorological variability on atmospheric chemistry. Our results also align with the results from
345 Garcia-Menendez et al. (2017), which recommended that simulations need to be at least 15 years
346 long to identify anthropogenically-forced ozone signals on the order of 1 ppbv.

347 Figures 4 and Supplemental Figures S1 and S2 compare the CASTNET observations to
348 the three CESM CAM-chem simulations, and while there are minor differences, there are broad
349 features that are consistent. First, using longer temporal averaging windows reduces the
350 influence of small-scale ozone variability at all spatial scales, and depending on the acceptable
351 threshold, one can select a temporal scale that effectively reduces the likelihood of exceeding
352 that threshold to zero. Second, larger spatial scales also reduce this likelihood of exceeding a
353 given threshold, but not as effectively as longer temporal scales. Finally, the impact of both
354 temporal and spatial averaging on ozone variability is largely consistent for the CASTNET
355 observations and for all three CESM CAM-chem simulations.

356

357 **3.3 Selection of Temporal Averaging Scales**

358 Figure 5 extends this analysis to examine the spatial heterogeneity of this likelihood of
359 exceeding particular thresholds at the grid cell level. Here we plot four thresholds (0.5, 1, 2.5,
360 and 5 ppbv) and four averaging windows (1, 5, 10, and 20 years) for the MOZ_2000 simulation.
361 Ozone variability is highest in the Eastern US. At the grid-cell level, there are two strategies for
362 filtering out the noise associated with natural meteorological variability (and thus enhancing
363 signal detection capabilities): either average over longer periods, or increase the threshold. For
364 these data, it is virtually certain that any 20-year average will be within 5 ppbv of a full 25-year
365 mean value (which itself may not be an accurate representation of a longer simulation), and
366 virtually certain that any 1-year average will be at least 0.5 ppbv away from the mean.

367 Figure 6 and Supplemental Figure S3 compare the MOZ_2000, MOZ_2050, and
368 MOZ_2100 simulations by selecting one column (the 5-year averaging window) and one row
369 (the 1 ppbv ozone threshold) from Figure 6 for MOZ_2000 to equivalent plots for MOZ_2050
370 and MOZ_2100. Interpreting Figures 7 and Supplemental Figure S3 give largely consistent



371 interpretations than the analysis above. Namely, that at the grid-scale level, increasing the
372 temporal averaging window (Figure 6) or increasing the acceptable ozone threshold
373 (Supplemental Figure S3) are effective at reducing the impact of the meteorological variability
374 on estimates of the ozone signal. Short windows (or smaller thresholds) are needed in the
375 Western US than in the Eastern US, and grid-cells over coastal and highly populated regions tend
376 to need longer windows (or higher thresholds). Finally, the 1 ppbv threshold and the 5-year
377 averaging window plots (in either Figure 5 or Supplemental Figure S3) indicate that the spatial
378 distribution and location of the peak variability may shift into the future, although this may be
379 due to parametric differences between MOZ_2000, MOZ_2050, and MOZ_2100. Future
380 simulations will be needed to check this shift in peak ozone variability.

381

382 **3.4 Selection of Spatial Averaging Scales**

383 We examine the impact of increasing the spatial averaging region (Figure 7) at four
384 different temporal averaging windows (1, 5, 10, and 20 years) and for the smallest ozone
385 threshold from the previous section (0.5 ppbv). It is evident that at all temporal averaging
386 windows, expanding the number of surrounding grid cells that are averaged together consistently
387 decreases the likelihood of exceeding the 0.5 ppbv threshold, although these reductions are
388 relatively small at the 1-year window, especially over the Eastern U.S. While increasing the
389 spatial averaging from a single grid-cell up to include the surrounding 81 grid cells (bottom row
390 in Figure 7) manages to essentially smooth away much of the spatial heterogeneity in surface
391 ozone (by moving down any column in Figure 7), it does not eliminate the likelihood of
392 exceeding the 0.5 ppbv threshold over much of the Eastern U.S. For instance, even at a 20-year
393 averaging window, and by averaging together the surrounding 81 grid-cells over locations in the
394 Eastern U.S., there is still a 20-70% likelihood of exceeding the 0.5 ppbv threshold due to the
395 small-scale impact of the meteorological variability on atmospheric chemistry.

396

397 **3.5 Combination of Spatial and Averaging Scales**

398 We now examine the combined impact of temporal and spatial averaging on reducing the
399 influence of small-scale ozone variability in order to enhance ozone signal detection capabilities.
400 Table S2 summarizes our analysis by dividing the likelihood of the ozone variability estimates
401 exceeding selected thresholds away from the long-term mean into four categories: (1) the length



402 of the averaging window over which ozone is averaged (columns); (2) the magnitude of the
403 ozone threshold of interest (rows); (3) the observed (CASTNET) and modeled (MOZ_2000,
404 MOZ_2050, and MOZ_2100) ozone data (sub-columns); and (4) the size of the spatial extent
405 over which ozone is averaged (sub-rows). A graphical representation consistent with the data
406 presented in Table S2 is plotted in Figure 8 for the Continental US average and for three grid
407 cells that represent various cases. In each plot in Figure 8, by moving along columns from left to
408 right, we can see the influence of increasing the size of the temporal averaging window, and by
409 moving along rows (from the bottom to the top), we can see the influence of increasing the
410 spatial averaging scale. By taking in the entire plot as a whole, we can get a feel for the
411 combined influence of both temporal and spatial averaging. Supplemental Figure S4 contains a
412 plot for each grid cell in the Continental US.

413 On average within the Continental US, both temporal and spatial averaging are effective
414 at reducing the calculated DM8H O₃ anomaly, although temporal averaging is more effective
415 (Figure 8a). There are many grid cells in the Eastern and Western US coasts (Figure 8b,
416 Supplemental Figure S4), where both spatial and temporal averaging are effective, but their
417 combined usage is especially effective. There are also many grid cells where temporal averaging
418 is effective, but spatial averaging is barely effective, or not effective at all (Figure 8c and
419 Supplemental Figure S4). Finally, there are some grid cells, particularly in the Central US
420 (Figure 8d and Supplemental Figure S4), where spatial averaging over smaller regions is
421 effective, but spatial averaging of larger regions actually increases the calculated DM8H O₃
422 anomaly by including surrounding grid cells that have higher variability.

423

424 **4 Discussion**

425 We now return to the original three research questions posed in Section 1. First, what is
426 the magnitude of ozone variability due to meteorology alone at the smallest scale, and what is the
427 impact of increasing the scale of temporal and spatial averaging? In both observed and modeled
428 DM8H O₃ surface data, the small-scale variability driven solely by the meteorological variability
429 impact on atmospheric chemistry (expressed as the standard deviation as a percentage of the
430 mean) can exceed 20% (Table 1, Figure 2d). The chemical variability examined here is the result
431 of fluctuations in meteorology, which itself results from larger-scale climatological drivers.
432 While variability in emissions also influences atmospheric chemistry, our analysis has removed



433 the influence of emissions variability and isolated the variability due to meteorology. There is
434 high temporal and spatial heterogeneity of surface ozone (Figure 2d), with the lowest values
435 found in the Western US (< 10%), higher values found in the Eastern US (up to 20%), and the
436 highest values over coastal or heavily populated regions (up to 30%). Averaging over longer
437 temporal scales (by increasing the averaging window) and over larger spatial scales (by
438 expanding the averaging region) can reduce the magnitude of the calculated variability, with
439 temporal averaging proving to be more effective than spatial averaging in most cases (Figure 8).
440 In this study, we performed simple spatial averaging, but there are other methodologies for
441 smoothing two-dimensional signals (e.g. Räisänen et al., 2011; Pogson and Smith, 2015) that
442 could potentially increase signal detection capabilities.

443 Second, are there combinations of temporal and spatial averaging that maximize the
444 filtration of calculated ozone variability, and thus maximize the potential for signal detection?
445 Figure 8 (and Supplemental Figure S4) demonstrate clearly that there are cases in which the
446 combined usage of temporal and spatial averaging can reduce the calculated variability better
447 than either strategy alone (see Figure 8b), although there are many regions within the Eastern US
448 in which spatial averaging has little to no impact on reducing the calculated variability (Figure
449 8c) or even results in an increase in the calculated variability (Figure 8d). There are no such
450 cases (see Supplemental Figure S4) in which expanding the temporal averaging scale increases
451 the calculated ozone variability. This could potentially enable region-specific averaging
452 strategies that help decision-makers identify and meet regional air quality objectives.

453 Third, are these results dependent on the particular parameterizations of the CESM
454 CAM-chem model, are they consistent with the available CASTNET observations? The three
455 CESM CAM-chem simulations exhibited consistent representations of ozone variability,
456 consistent with our understanding of future changes to the climate (and meteorology) and the
457 resulting impact on atmospheric chemistry (Table 1, Figure 4, S1, and S2). Compared to the
458 CASTNET observations (which we detrended to remove the influence of changing precursor
459 emissions), the present-day simulation (MOZ_2000) exhibited a high ozone bias in the Eastern
460 US (which is also evident in the future simulations, MOZ_2050 and MOZ_2100), while the
461 representation of the ozone variability is comparable (Table 1).

462 Finally, how may these strategies be applied to other datasets, be they chemical,
463 meteorological, or climatological? Much of this analysis could be applied to any dataset that has



464 spatial and temporal coverage, as long as some set of acceptable thresholds is provided. While
465 our time step in this analysis is daily (given the DM8H O₃ metric), and applied only to
466 summertime (JJA) days, any time step (i.e. hourly, monthly, annual, decadal) could be utilized as
467 long as cyclical trends (e.g. diurnal or seasonal cycles) are removed. Indeed, the sliding-scale
468 presentation in Figure 8 and Supplemental Figure S4 can specifically be utilized to identify
469 particular spatial and temporal scales that are sufficient to identify signals at particular thresholds
470 and to identify particular geographic regions that are best suited to identify a given signal. For
471 example, Sofen et al. (2016) identified regions across the globe where additional observations
472 would be particularly suited to improve our understanding of surface ozone behavior, and our
473 analysis could potentially be used to identify particular temporal and spatial averaging scales that
474 could further maximize the capability for trend detection. In particular, Sofen et al. (2016) noted
475 that the peak in the power spectrum of the El Niño-Southern Oscillation (ENSO) on surface
476 ozone is at the 3.8 year time scale, and that within some regions within the US, the amplitude of
477 the ENSO influence on surface ozone approached 0.5 ppbv (and up to 1.1 ppbv globally). Our
478 analysis shows that there are no grid cells within the Continental US where a 0.5 ppbv signal can
479 be identified at the 5-year (or shorter) temporal averaging scale (Supplemental Figure S4), but
480 that there are many regions – especially within the Western US – in which even a modest amount
481 of spatial averaging can identify surface ozone signals below the 1 ppbv level with a 5-year or
482 shorter averaging window. The type of sliding-scale analysis – in which spatial and temporal
483 averaging are utilized individually and in combination – as presented in Figure 8 and
484 Supplemental Figure S4 could readily be applied to a wide range of atmospheric (and other)
485 topics to aid in the capability to identify signals that exist both in space and in time. In particular,
486 low-frequency oscillations (e.g. ENSO, and others) and other forms of internally or externally
487 forced trends (e.g. anthropogenic and natural changes in emissions) are readily adaptable to this
488 type of analysis.

489 Finally, we did not quantify statistical significance (as in Lewandowski et al., 2015) as
490 our goals were to understand the general nature of ozone variability at all scales and for all signal
491 strengths. Statistical significance testing (and other statistical techniques) can certainly provide
492 additional information as to the strengths of ozone signals within the underlying variability, and
493 can be used to extend these results in a case-by-case manner, but we leave this testing to future
494 studies that can focus on particular air quality objectives at particular temporal and spatial scales.



495

496 **5 Conclusions**

497 We quantified the impact of spatial and temporal averaging at different scales – both
498 individually and combined – on estimates of surface ozone variability and the resulting
499 likelihood of over-confidence in estimates of chemical signals over the United States using
500 CASTNET observations and the CESM CAM-chem model. We simulate three multi-decadal
501 time periods, each with constant surface emissions, and find that this analysis is consistent across
502 our simulated time periods, and that our results are not sensitive to particular configurations
503 parametric choices within the CESM CAM-chem (i.e. emissions, meteorology, and climate). We
504 also provide a conceptual framework for gaining understanding of the influence of spatial and
505 temporal averaging that may be adapted to a wide range of atmospheric and surface phenomena,
506 provided sufficient spatial and temporal coverage. Here we focus on surface ozone, a highly
507 variable (in both space and time) atmospheric constituent with severe human health impacts and
508 implications for planetary climate, which is the focus of many local, regional, and national
509 policies. However, the resultant magnitude of these changes and trends are small compared to the
510 magnitude of the day-to-day ozone variability, and detecting these changes and trends can be
511 challenging. Our analysis and conceptual framework allow for a selection of spatial and temporal
512 averaging scales that can aid in this signal detection.

513 In order to quantify the impact of spatial and temporal averaging on ozone variability, we
514 start by selecting four telescoping spatial regions (the Continental US, the Eastern US, the
515 Northeastern US, and a single grid cell within the Northeastern US) and examine all possible
516 choices for averaging windows (ranging from daily to multi-decadal windows), although we
517 focused primarily on averaging windows of 1, 5, 10, and 20 years. We find that – consistent with
518 previous studies – ozone variability is largest at the smallest scales, and is frequently on the order
519 of $\pm 10 - 20$ ppbv, or which is roughly 15-20% of the mean ozone signal. In order to minimize
520 the chemical noise that results from meteorological variability – and thus enhance the signal –
521 we find averaging windows of 10-15 years (and sometimes longer at the smaller spatial scales)
522 combined with modest (nearest-neighbor) spatial averaging substantially improve the capability
523 for trend detection.

524 We show that the largest ozone variability is found in the Eastern US (Figure 5, Figure S4),
525 and subsequently there are many regions within the Eastern US where even a 20-year averaging



526 window has a non-negligible likelihood of estimating ozone variability that is dependent (with
527 possible error in the 1 – 3 ppbv range) on the particular years selected. In addition, over much of
528 the Eastern US, simulations of 5-years or shorter have a substantial likelihood (40 – 90%,
529 Figures S1 and S2) of reflecting the influence of meteorological variability on chemistry rather
530 than the mean state of surface ozone, with the possibility of 5 – 10 ppbv error (Figure S4).

531 Finally, we demonstrate a conceptual framework that allows for a “sliding-scale” view of
532 surface ozone variability, in which both temporal and spatial averaging is examined at every grid
533 cell within the Continental US. We show that the magnitude of estimates of ozone variability can
534 be reduced with both temporal and spatial averaging, although temporal averaging tends to be
535 more effective. While there are many regions in which both temporal and spatial averaging used
536 in conjunction substantially reduce the estimate of ozone variability, there are some regions
537 where spatial averaging is ineffective, or even counter-effective. In contrast, this is not the case
538 for temporal averaging, which consistently reduces the magnitude of estimated ozone variability.
539 Our analysis could be combined with other studies (e.g. Sofen et al., 2016) to guide
540 observational and modeling strategies and identify regions and scales at which particular signals
541 are most likely to be identified.

542



543 **Code Availability**

544 CESM CAM-Chem code is available through the National Center for Atmospheric Research /
545 University Corporation for Atmospheric Research (NCAR/UCAR) website
546 (<http://www.cesm.ucar.edu/models/cesm1.2/>), and this project made no code modifications from
547 the released model version.



548 **Data Availability**

549 The raw model output is archived on the NCAR servers, and processed data will be made

550 available upon publication on Massachusetts Institute of Technology servers.



551 **Supplemental Link**

552



553 **Author Contribution**

554 BBS ran the present-day simulation, analyzed the data, and wrote the manuscript. FGM ran the
555 future simulations and made the data available to BBS. NS, RP, EM, ST, and LE guided and
556 reviewed the scientific modeling and analysis process, and provided feedback throughout the
557 project and development of the manuscript.

558



559 **Competing Interests**

560 The authors declare that they have no conflict of interest.

561



562 **Acknowledgements**

563 This model development work was supported by the U.S. Department of Energy (DOE) Grant
564 DE-FG02-94ER61937 to the MIT Joint Program on the Science and Policy of Global Change.
565 Computational resources for this project were provided by DOE and a consortium of other
566 government, industry, and foundation sponsors of the Joint Program. For a complete list of
567 sponsors, see: <http://globalchange.mit.edu>. Additional computing resources were provided by the
568 Climate Simulation Laboratory at NCAR's Computational and Information Systems Laboratory
569 (CISL), sponsored by the National Science Foundation and other agencies. The National Center
570 for Atmospheric Research is funded by the National Science Foundation. The authors would also
571 like to thank Daniel Rothenberg for efficient processing of the ozone files.

572

573 **References**

- 574 Angélic, O., Stone, D., Perkins-Kirkpatrick, S., Alexander, L. V., Wehner, M., Shiogama, H.,
575 Wolski, P., Ciavarella, A., and Christidis, N.: On the nonlinearity of spatial scales in
576 extreme weather attribution statements, *Clim. Dyn.*, 2017.
- 577 Barnes, E. A., Fiore, A. M., and Horowitz, L. W.: Detection of trends in surface ozone in the
578 presence of climate variability, *J. Geophys. Res. Atmos.*, 121, 6112–6129, 2016.
- 579 Brown-Steiner, B., Hess, P. G., and Lin, M. Y.: On the capabilities and limitations of GCCM
580 simulations of summertime regional air quality: A diagnostic analysis of ozone and
581 temperature simulations in the US using CESM CAM-chem, *Atmos. Environ.*, 101, 134–
582 148, 2015.
- 583 Cooper, O. R., Gao, R. S., Tarasick, D., Leblanc, T., and Sweeney, C.: Long-term ozone trends
584 at rural ozone monitoring sites across the United States, 1990-2010, *J. Geophys. Res.*, 117,
585 D22307, 2012.
- 586 de Elía, R., Biner, S., and Frigon, A.: Interannual variability and expected regional climate
587 change over North America, *Clim. Dyn.*, 41, 1245, 2013.
- 588 Deser, C., Phillips, A., Bourdette, V., and Teng, H.: Uncertainty in climate change projections:
589 the role of internal variability, *Clim. Dyn.*, 38, 527, 2012.
- 590 Diem, J. E., and Comrie, A. C.: Predictive mapping of air pollution involving sparse spatial
591 observations, *Environmental Pollution*, 119, 1, 99–117, 2002.
- 592 Emmons, L. K., Walters, S., Hess, P. G., Lamarque, J.-F., Pfister, G. G., Fillmore, D., Granier,
593 C., Guenther, A., Kinnison, D., Laepple, T., Orlando, J., Tie, X., Tyndall, G., Wiedinmyer,
594 C., Baughcum, S. L., and Kloster, S.: Description and evaluation of the Model for Ozone
595 and Related chemical Tracers, version 4 (MOZART-4), *Geosci. Model Dev.*, 3, 43-67,
596 2010.
- 597 Fiore, A. M., Oberman, J. T., Lin, M. Y., Zhang, L., Clifton, O. E., Jacob, D. J., Naik, V.,
598 Horowitz, L. W., Pinto, J. P., and Milly, G. P.: Estimating North American background
599 ozone in U.S. surface air with two independent global models: Variability, uncertainties,
600 and recommendations, *Atmos. Environ.*, 96, 284–300, 2014.
- 601 Fiore, A. M., Jacob, D. J., Liu, H., Yantosca, R. M., Fairlie, T. D., and Li, Q.: Variability in
602 surface ozone background over the United States: Implications for air quality policy, *J.*
603 *Geophys. Res. Atmos.*, 108, D24, 1787, 2003.
- 604 Garcia-Menendez, F., Saari, R. K., Monier, E., and Selin, N. E.: U.S. Air Quality and Health
605 Benefits from Avoided Climate Change under Greenhouse Gas Mitigation, *Environ. Sci.*
606 *Technol.*, 49, 7580–7588, 2015.
- 607 Garcia-Menendez, F., Monier, E., and Selin, N. E.: The role of natural variability in projections
608 of climate change impacts on U.S. ozone pollution, *Geophys. Res. Lett.*, 44, 2911–2921,
609 2017.
- 610 Giorgi, F., and Bi, X.: Time of emergence (TOE) of GHG-forced precipitation change hot-spots,
611 *Geophys. Res. Lett.*, 36, L06709, 2009.



- 612 Guenther, A. B., Jiang, X., Heald, C. L., Sakulyanontvittaya, T., Duhl, T., Emmons, L. K., and
613 Wang, X.: The Model of Emissions of Gases and Aerosols from Nature version 2.1
614 (MEGAN2.1): An extended and updated framework for modeling biogenic emissions,
615 *Geosci. Model Dev.*, 5, 1471–1492, 2012.
- 616 Hawkins, E., and Sutton, R.: Time of emergence of climate signals, *Geophys. Res. Lett.*, 39,
617 L01702, 2012.
- 618 Jacob, D. J., and Winner, D. A.: (2009). Effect of climate change on air quality, *Atmos. Environ.*,
619 43, 51–63, 2009.
- 620 Jhun, I., Coull, B. A., Schwartz, J., Hubbell, B., and Koutrakis, P.: The impact of weather
621 changes on air quality and health in the United States in 1994–2012, *Environ. Res. Lett.*, 10,
622 084009, 2015.
- 623 Kay, J. E., Deser, C., Phillips, A., Mai, A., Hannay, C., Strand, G., Arblaster, J. M., Bates, S. C.,
624 Danabasoglu, G., Edwards, J., Holland, M., Kushner, P., Lamarque, J.-F., Lawrence, D.,
625 Lindsay, K., Middleton, A., Munoz, E., Neale, R., Oleson, K., Polvani, L., and Vertenstein,
626 M.: The Community Earth System Model (CESM) large ensemble project: A community
627 resource for studying climate change in the presence of internal climate variability, *Bull.*
628 *Amer. Meteor. Soc.*, 96, 1333–1349, 2015.
- 629 King, A. D., Donat, M. G., Fischer, E. M., Hawkins, E., Alexander, L. V., Karoly, D. J., Dittus,
630 A. J., Lweis, S. C., and Perkins, S. E.: The timing of anthropogenic emergence in simulated
631 climate extremes, *Environ. Res. Lett.*, 10, 094015, 2015.
- 632 Knote, C., Tuccella, P., Curci, G., Emmons, L., Orlando, J. J., Madronich, S., Baró, R., Joménez-
633 Guerrero, P., Luecken, D., Hogrefe, C., Forkel, R., Werhahn, J., Hirtl, M., Pérez, J. L., José,
634 R. S., Giordano, L., Brunner, D., Yahya, K., and Zhang, Y.: Influence of the choice of gas-
635 phase mechanism on predictions of key gaseous pollutants during the AQMEII phase-2
636 intercomparison, *Atmos. Environ.*, 115, 553–568, 2015.
- 637 Knutti, R.: The end of model democracy?, *Clim. Change*, 102, 395–404, 2010.
- 638 Lamarque, J.-F., Bond, T. C., Eyring, V., Granier, C., Heil, A., Klimont, Z., Lee, D., Lioussé, C.,
639 Mieville, A., Owen, B., Schultz, M. G., Shindell, D., Smith, S. J., Stehfest, E., Van
640 Aardenne, J., Cooper, O. R., Kainuma, M., Mahowald, N., McConnell, J. R., Naik, V.,
641 Riahi, K., and Van Vuuren, D. P.: Historical (1850–2000) gridded anthropogenic and
642 biomass burning emissions of reactive gases and aerosols: Methodology and application,
643 *Atmos. Chem. Phys.*, 10, 7017–7039, 2010.
- 644 Lamarque, J.-F., Dentener, F., McConnell, J., Ro, C.-U., Shaw, M., Vet, R., Bergmann, D.,
645 Cameron-Smith, P., Dalsoren, S., Doherty, R., Faluvegi, G., Ghan, S. J., Josse, B.,
646 MacKenzie, I. A., Plummer, D., Shindell, D. T., Skeie, R. B., Stevenson, D. S., Strode, S.,
647 Zeng, G., Curran, M., Dahl-Jensen, D., Das, S., Fritzsche, D., and Nolan, M.: Multi-model
648 mean nitrogen and sulfur deposition from the atmospheric chemistry and climate model
649 intercomparison project (ACCMIP): Evaluation of historical and projected future changes,
650 *Atmos. Chem. Phys.*, 13, 7997–8018, 2013.
- 651 Lamarque, J.-F., Emmons, L. K., Hess, P. G., Kinnison, D. E., Tilmes, S., Vitt, F., Heald, C. L.,
652 Holland, E. A., Lauritzen, P. H., Neu, J., Orlando, J. J., Rasch, P. J., and Tyndall, G. K.:



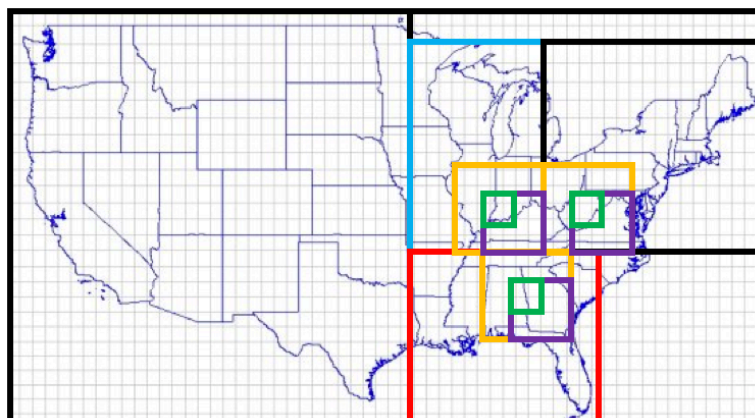
- 653 CAM-chem: Description and evaluation of interactive atmospheric chemistry in the
654 Community Earth System Model, *Geosci. Model Dev.*, 5, 369–411, 2012.
- 655 Lawrence, M. G., Hov, Ø., Beekmann, M., Brandt, J., Elbern, H., Eskes, H., Feichter, H., and
656 Takigawa, M.: The chemical weather, *Environ. Chem.*, 2, 6–8, 2005.
- 657 Lewandowsky, S., Risbey, J. S., and Oreskes, N.: On the definition and identifiability of the
658 alleged “hiatus” in global warming, *Sci. Rep.*, 5, 16784, 2015.
- 659 Lin, M., Horowitz, L. W., Oltmans, S. J., Fiore, A. M., and Fan, S.: Tropospheric ozone trends at
660 Mauna Loa Observatory tied to decadal climate variability, *Nat. Geosci.*, 7, 136–143, 2014.
- 661 McComiskey, A., and Feingold, G.: The scale problem in quantifying aerosol indirect effects,
662 *Atmos. Chem. Phys.*, 12, 1031–1049, 2012.
- 663 Medhaug, I., Stolpe, M. B., Fischer, E. M., and Knutti, R.: Reconciling controversies about the
664 ‘global warming hiatus,’ *Nature*, 545, 41–47, 2017.
- 665 Möller, D. *Chemistry of the Climate System*, pp. 331–334, Walter de Gruyter GmbH and Co.,
666 KG, Berlin/New York, 2010.
- 667 Monier, E., Scott, J. R., Sokolov, A. P., Forest, C. E., and Schlosser, C. A.: An integrated
668 assessment modeling framework for uncertainty studies in global and regional climate
669 change: The MIT IGSM-CAM (version 1.0), *Geosci. Mod. Dev.*, 6, 2063–2085, 2013.
- 670 Monier, E., Gao, X., Scott, J. R., Sokolov, A. P., and Schlosser, C. A.: A framework for
671 modeling uncertainty in regional climate change, *Clim. Change*, 131, 51–66, 2015.
- 672 Monier, E., Xu, L., and Snyder, R.: Uncertainty in future agro-climate projections in the United
673 States and benefits of greenhouse gas mitigation, *Environ. Res. Lett.*, 11, 055001, 2016.
- 674 Paltsev, S., Reilly, J. M., Jacoby, H. D., Eckaus, R. S., McFarland, J. R., Sarofim, M. C.,
675 Asadoorian, M. O., and Babiker, M. H.: The MIT emissions prediction and policy analysis
676 (EPPA) model: Version 4, Rep. 125, MIT Joint Program on the Sci. and Policy of Global
677 Change, 2005.
- 678 Pogson, M., and Smith, P.: Effect of spatial data resolution on uncertainty, *Environ. Model.*
679 *Softw.*, 63, 87–96, 2015.
- 680 Pyle, J. A., and Zavody, A. M.: The modelling problems associated with spatial averaging, *Q. J.*
681 *R. Meteorol. Soc.*, 116, 753–766, 1990.
- 682 Räisänen, J., and Ylhäisi, J. S.: How much should climate model output be smoothed in space?,
683 *J. Climate*, 24, 867–880, 2011.
- 684 Rasmussen, D. J., Fiore, A. M., Naik, V., Horowitz, L. W., McGinnis, S. J., and Schultz, M. G.:
685 Surface ozone-temperature relationships in the eastern US: A monthly climatology for
686 evaluating chemistry-climate models, *Atmos. Environ.*, 47, 142–153, 2012.
- 687 Rienecker, M. M., Suarez, M. J., Gelaro, R., Todling, R., Bacmeister, J., Liu, R., Bosilovich, M.
688 G., Schubert, S. D., Takacs, L., Kim, G-K, Bloom, S., Chen, J., Collins, D., Conaty, A., da
689 Silva, A., Gu, W., Joiner, J., Koster, R. D., Lucchesi, R., Molod, A., Owens, T., Pawson, S.,
690 Pegion, P., Redder, C. R., Reichle, R., Robertson, F. R., Ruddick, A. G., Sienkiewicz, M.,
691 and Woollen, J.: MERRA: NASA’s Modern-Era Retrospective analysis for Research and
692 Applications, *J. Climate*, 24, 3624–3648, 2011.



- 693 Roberts, C. D., Palmer, M. D., McNeall, D., and Collins, M.: Quantifying the likelihood of a
694 continued hiatus in global warming, *Nat. Clim. Change*, 5, 337–342, 2015.
- 695 Schnell, J. L., and Prather, M. J.: Co-occurrence of extremes in surface ozone, particulate matter,
696 and temperature over eastern North America, *Proc. Natl. Acad. Sci. U.S.A.*, 114, 11, 2854–
697 2859, 2017.
- 698 Schurer, A. P., Hegerl, G. C., Mann, M. E., Tett, S. F. B., and Phipps, S. J.: Separating forced
699 from chaotic climate variability over the past millennium, *J. Climate*, 26, 6954–6973, 2013.
- 700 Searle, K. R., Chipperfield, M. P., Bekki, S., and Pyle, J. A.: The impact of spatial averaging on
701 calculated polar ozone loss: 2. Theoretical analysis, *J. Geophys. Res.*, 103, D19, 25409–
702 25416, 1998.
- 703 Sofen, E. D., Bowdalo, D., and Evans, M. J.: How to most effectively expand the global surface
704 ozone observing network, *Atmos. Chem. Phys.*, 16, 1445–1457, 2016.
- 705 Stevenson, D. S., Young, P. J., Naik, V., Lamarque, J. F., Shindell, D. T., Voulgarakis, A., Skeie,
706 R. B., Dalsøren, S. B., Myhre, G., Berntsen, T. K., Folberth, G. A., Rumbold, S. T., Collins,
707 W. J., MacKenzie, I. A., Doherty, R. M., Zeng, G., van Noije, T. P. C., Strunk, A.,
708 Bergmann, D., Cameron-Smith, P., Plummer, D. A., Strode, S. A., Horowitz, L., Lee, Y. H.,
709 Szopa, S., Sudo, K., Nagashima, T., Josse, B., Cionni, I., Righi, M., Eyring, V., Conley, A.,
710 Bowman, K. W., and Wild, O.: Tropospheric ozone changes, radiative forcing and
711 attribution to emissions in the Atmospheric Chemistry and Climate Model Intercomparison
712 Project (ACCMIP), *Atmos. Chem. Phys.*, 13, 3063–3085, 2013.
- 713 Sun, J., Fu, J. S., Drake, J., Lamarque, J.-F., Tilmes, S., and Vitt, F.: Improvement of the
714 prediction of surface ozone concentration over conterminous U.S. by a computationally
715 efficient second-order Rosenbrock solver in CAM4-Chem, *J. Adv. Model Earth. Sy.*, 9,
716 482–500, 2017.
- 717 Tilmes, S., Lamarque, J.-F., Emmons, L. K., Conley, A., Schultz, M. G., Saunio, M., Thouret,
718 V., Thompson, A. M., Oltmans, S. J., Johnson, B., and Tarasick, D.: Technical Note:
719 Ozonesonde climatology between 1995 and 2011 : description, evaluation and applications,
720 *Atmos. Chem. Phys.*, 12, 7475–7497, 2012.
- 721 Tilmes, S., Lamarque, J. F., Emmons, L. K., Kinnison, D. E., Ma, P. L., Liu, X., Ghan, S.,
722 Bardeen, C., Arnold, S., Deeter, M., Vitt, F., Ryerson, T., Elkins, J. W., Moore, F.,
723 Spackman, J. R., and Val Martin, M.: Description and evaluation of tropospheric chemistry
724 and aerosols in the Community Earth System Model (CESM1.2), *Geosci. Model Dev.*, 8,
725 1395–1426, 2015.
- 726 Tilmes, S., Lamarque, J. F., Emmons, L. K., Kinnison, D. E., Marsh, D., Garcia, R. R., Smith, A.
727 K., Neely, R. R., Conley, A., Vitt, F., Val Martin, M., Tanimoto, h., Simpson, I., Blake, D.
728 R., and Blake, N.: Representation of the Community Earth System Model (CESM1) CAM4-
729 chem within the Chemistry-Climate Model Initiative (CCMI), *Geosci. Model Dev.*, 9,
730 1853–1890, 2016.
- 731 Travis, K. R., Jacob, D. J., Fisher, J. A., Kim, P. S., Marais, E. A., Zhu, L., Yu, K., Miller, C. C.,
732 Yantosca, R. M., Sulprizio, M. P., Thompson, A. M., Wennberg, P. O., Crouse, J. D., St.
733 Clair, J. M., Cohen, R. C., Laughner, J. L., Dibb, J. E., Hall, S. R., Ullmann, K., Wolfe, G.
734 M., Pollack, I. B., Peischl, J., Neuman, J. A., and Zhou, X.: Why do models overestimate



- 735 surface ozone in the Southeast United States?, Atmos. Chem. Phys., 16, 13561–13577,
736 2016.
- 737 US EPA: National Ambient Air Quality Standards for Ozone: Final Rule. Fed. Regist. 80 (206),
738 65292-65468. 2015.
- 739 US EPA: CASTNET 2014 Annual Report Prepared by Environmental Engineering and
740 Measurement Services, Inc. for the U.S. Environmental Protection Agency, 2016.
- 741 Wild, O., and Prather, M. J.: Global tropospheric ozone modeling: Quantifying errors due to grid
742 resolution, J. Geophys. Res., 111, D11305, 2006.
- 743 Young, P. J., Archibald, A. T., Bowman, K. W., Lamarque, J.-F., Naik, V., Stevenson, D. S.,
744 Tilmes, S., Voulgarakis, A., Wild, O., Bergmann, D., Cameron-Smith, P., Cionni, I.,
745 Collins, W. J., Dalsøren, S. B., Doherty, R. M., Eyring, V., Faluvegi, G., Horowitz, L. W.,
746 Josse, B., Lee, Y. H., MacKenzie, I. A., Nagashima, T., Plummer, D. A., Righi, M.,
747 Rumbold, S. T., Skeie, R. B., Shindell, D. T., Strode, S. A., Sudo, K., Szopa, S., and Zeng,
748 G.: Pre-industrial to end 21st century projections of tropospheric ozone from the
749 Atmospheric Chemistry and Climate Model Intercomparison Project (ACCMIP), Atmos.
750 Chem. Phys., 13, 2063–2090, 2013.



751

752

753

754

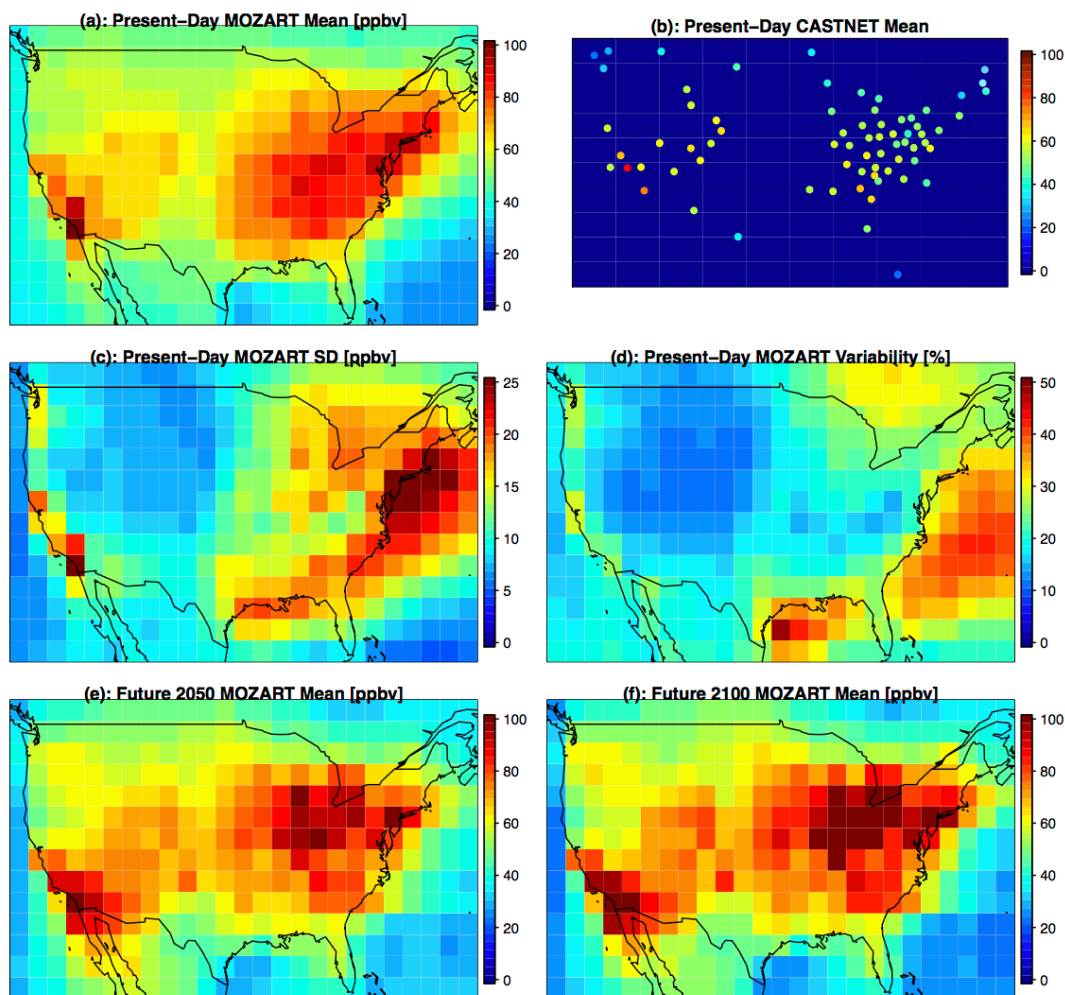
755

756

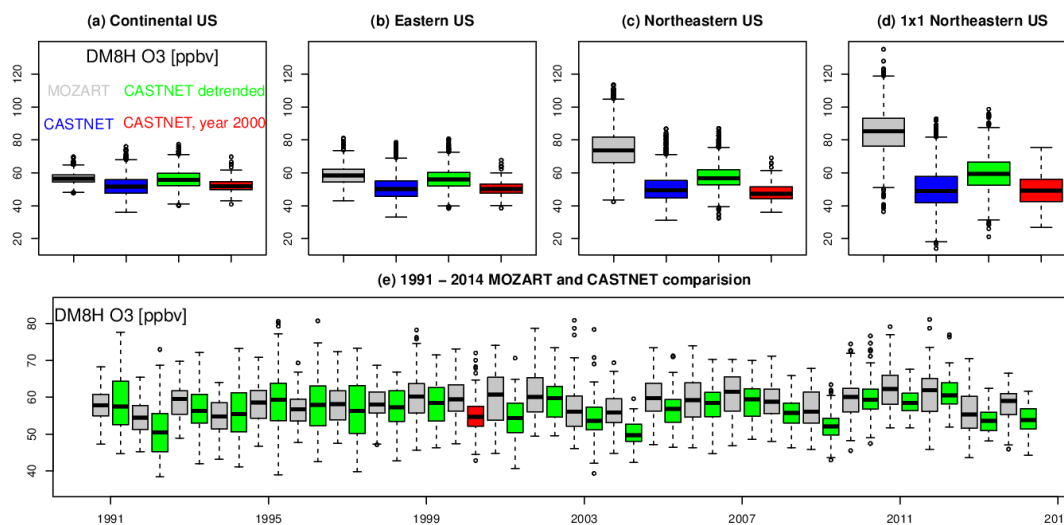
757

758

Figure 1: Telescoping Spatial Regions included in this study. The largest scale we consider is the Continental US (outer border). We focus on the Eastern US, by subdividing into three subregions: the Midwest (blue), Northeast (black), and Southeast (red). Within each subregion we telescope into a 3x3 grid cell (yellow), 2x2 grid cell (purple), and a 1x1 grid cell (green). In the paper, we only show a subset of these telescoping regions, and we include the rest in the Supplemental Material.

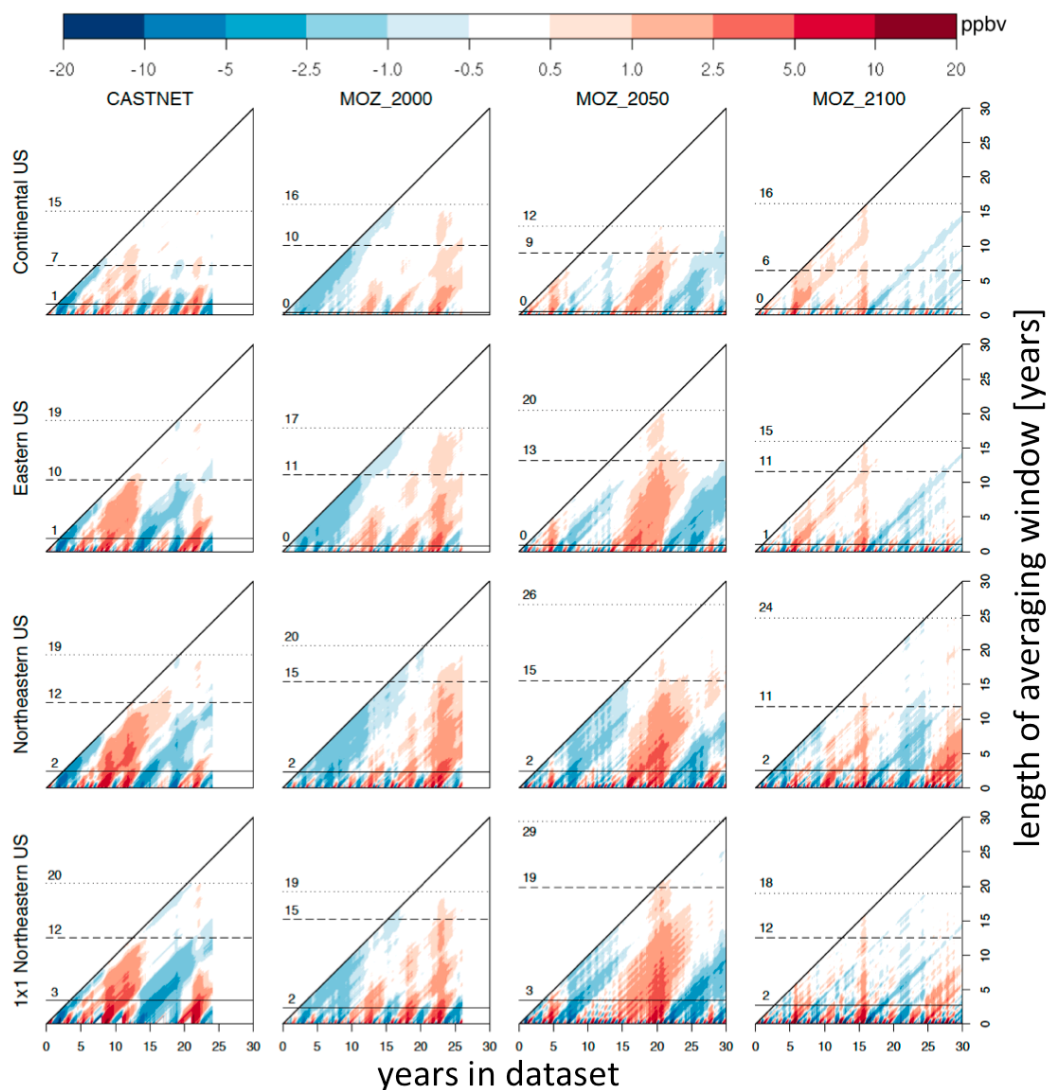


759
760
761 **Figure 2:** Continental US surface maps of (a) present-day MOZART mean DM8H O₃; (b) present-day
762 CASTNET mean DM8H O₃; (c) present-day MOZART standard deviation; (d) present-day MOZART
763 variability (standard deviation divided by mean, as a percent); (e) future MOZART year 2050 mean DM8H
764 O₃; and (f) future MOZART year-2100 mean DM8H O₃. All model results are averaged over every JJA day
765 in the time series, while the CASTNET results are only for the year 2000.



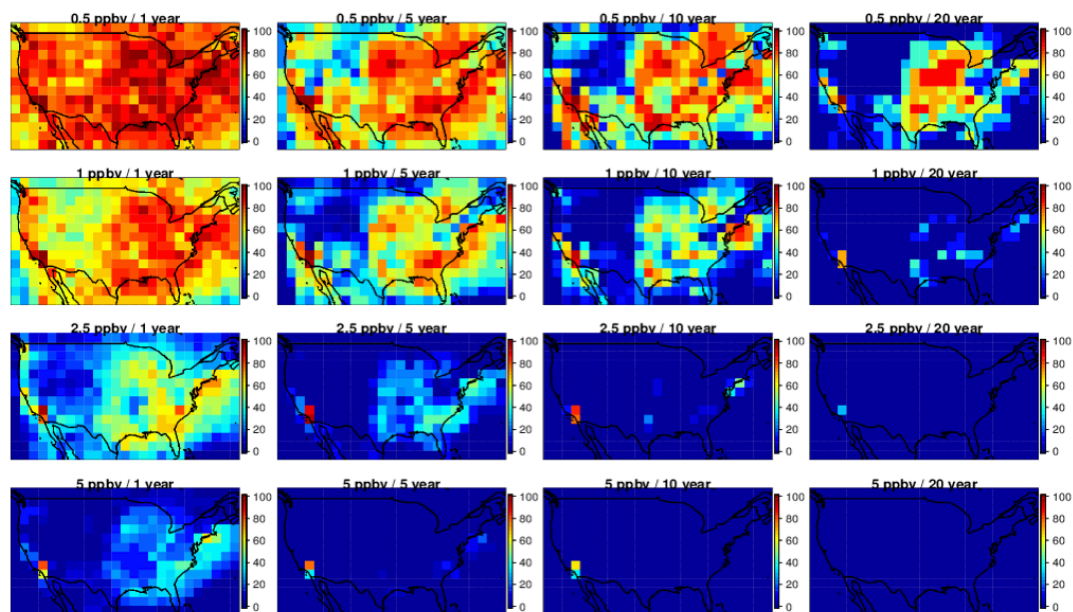
766
767
768
769
770
771
772
773
774
775
776
777
778

Figure 3: (a-d): Boxplots for surface DM8H O₃ for every summertime (JJA) day from 1991 – 2014 averaged over the Continental US, the Eastern US, the Northeastern US, and a single grid cell in the Northeastern US from CESM CAM-chem (grey), CASTNET observations (blue), detrended CASTNET observations (green), and the detrended CASTNET values for the year 2000 only (red). (e) Comparison of the yearly JJA DM8H O₃ estimates averaged over the Eastern US for MOZART (grey) and the detrended CASTNET (green) from 1991 – 2014. The single red boxplot coincides with the red boxplot in (b). The units are in ppbv, and for each boxplot the box contains the Inter Quartile Range (IQR), the horizontal line within the box is the median, and the whiskers extend out to the farthest point which is within 1.5 times the IQR with circles indicating any outliers.



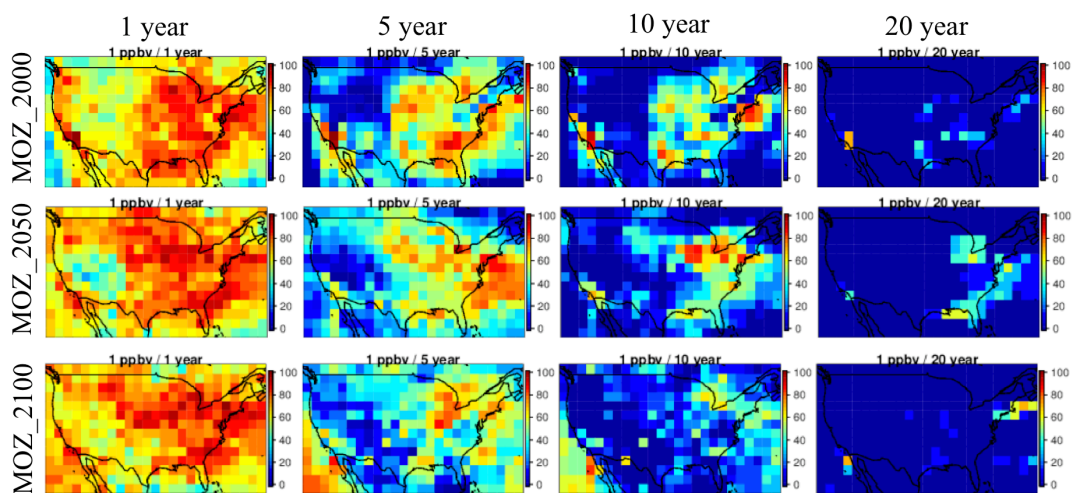
779
780
781
782
783
784
785
786
787
788
789
790
791

Figure 4: A representation of the variability of the DM8H O₃ anomaly (from the long-term mean) for the four datasets in this study (CASTNET, MOZ_2000, MOZ_2050, MOZ_2100, columns) averaged over the four telescoping regions (CUS, EUS, NEUS, NEUS 1x1, rows). In each panel, the horizontal axis is the number of years in the dataset (24 years (1991-2014) for CASTNET, 26 years (1990-2015) for MOZ_2000, and 30 years (2036-2065 and 2086-2115) for MOZ_2050 and MOZ_2100), and the vertical axis represents the length of the averaging window (ranging from 1 day (bottom row) up to the entire time series (top pixel)). Each pixel represents the estimate of the ozone anomaly for a given averaging window (vertical axis) ending at a given time (horizontal axis). Horizontal lines indicate the length of averaging window required to guarantee that the variability drops below thresholds of 5 ppbv (solid), 1 ppbv (dashed), and 0.5 ppbv (dotted).



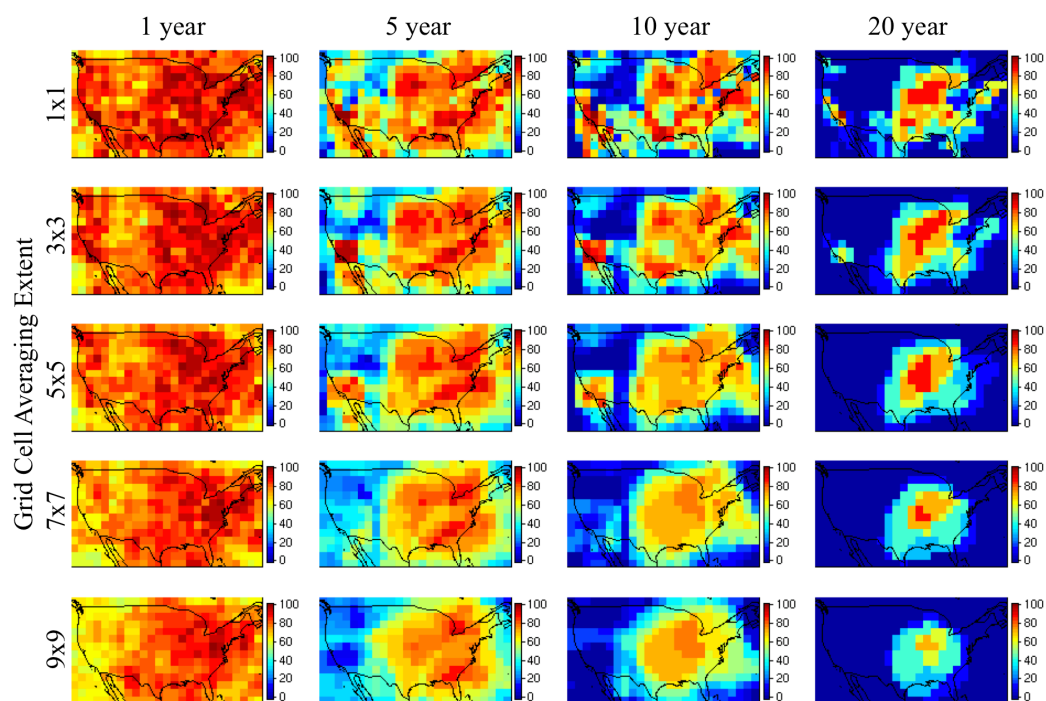
792
793
794
795
796

Figure 5: Spatial Plots over the Continental US plotting the likelihood (%) that an estimate of ozone exceeds a given threshold due to meteorological variability (rows) at the grid-cell level when using different lengths of averaging windows (columns) for the present-day CESM simulation (MOZ_2000).



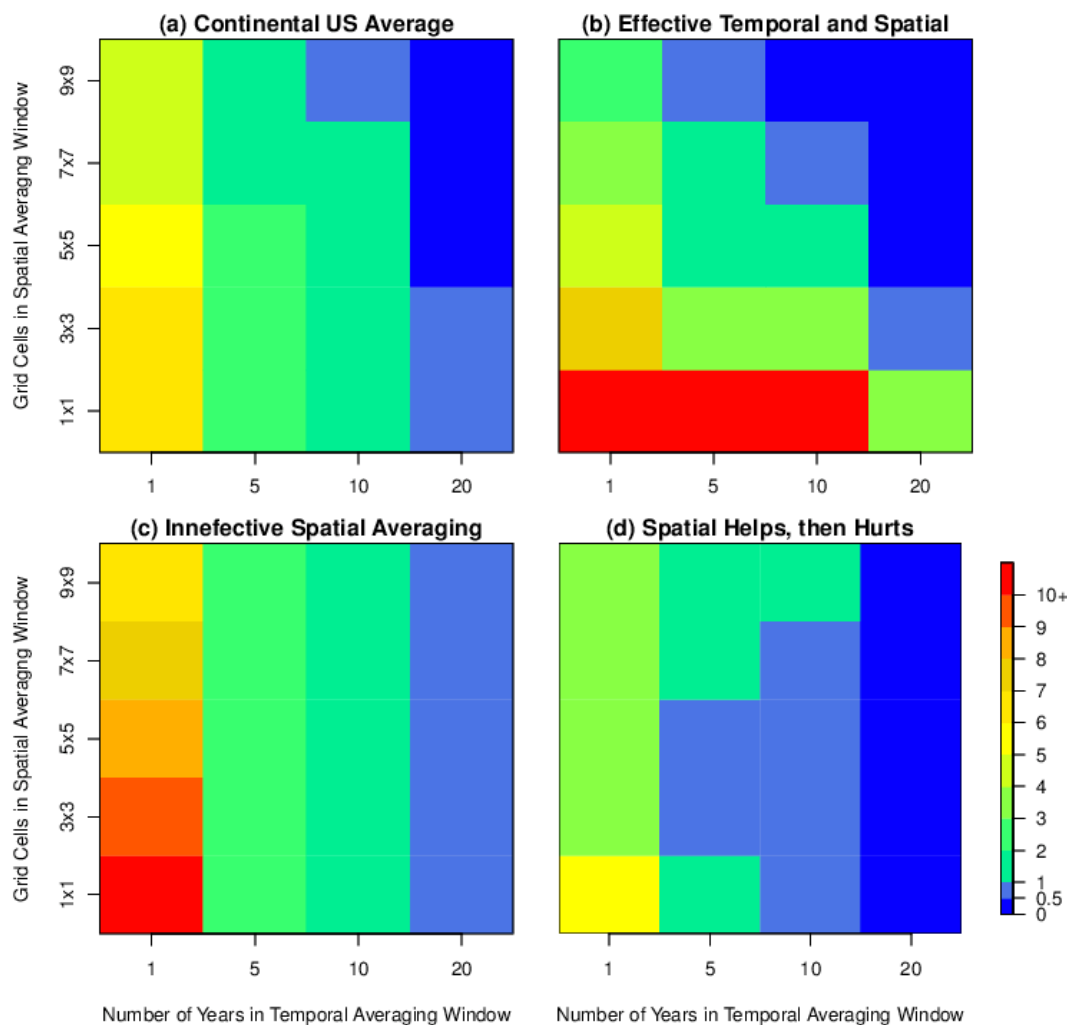
797
798
799
800

Figure 6: As in Figure 5, but only the second row, for present-day CAM-chem, future CAM-chem 2050, and future CAM-chem 2100.



801
802
803
804
805
806

Figure 7: Combined impact of temporal and spatial averaging on reducing ozone variability on the likelihood (%) of exceeding the 0.5 ppbv threshold (as in Figures 5, 6, and Supplemental Figure S3) for the present-day MOZ_2000 simulation. The top row is the same as in Figure 6, while the lower rows have averaged the values within a 3x3, 5x5, 7x7, and 9x9 box surrounding each individual grid cell.



807

808 **Figure 8: The maximum potential calculated DM8H O₃ anomaly [ppbv] from the long-term mean for (a)**
809 **the Continental US average and three individual grid cells taken from (b) Southern California, (c) the**
810 **Northeast, and (d) the Rocky Mountains demonstrating the impact of temporal and spatial averaging,**
811 **with the number of years included in the temporal averaging window increasing along the x-axis and the**
812 **number of grid cells included in the spatial averaging window increasing along the y-axis. A full map of**
813 **the Continental US can be found in the Supplemental Material (Figure S4). Note that the color scale is**
814 **non-linear, and the color transitions are selected to match the thresholds established throughout this**
815 **paper.**
816



		CASTNET	MOZ_2000	MOZ_2050	MOZ_2100	
Continental US	Mean	ppbv	52.4	56.7	56.8	57.4
	Standard Deviation	ppbv	5.04	3.08	3.54	3.73
	Variability	%	10%	5%	6%	7%
	Bias	ppbv		4.31		
Eastern US	Mean	ppbv	50.7	58.6	55.5	56.5
	Standard Deviation	ppbv	5.78	5.77	5.80	6.50
	Variability	%	11%	10%	10%	12%
	Bias	ppbv		7.91		
Northeastern US	Mean	ppbv	48.3	74.4	68.4	73.0
	Standard Deviation	ppbv	6.89	11.4	11.1	12.7
	Variability	%	14%	15%	16%	17%
	Bias	ppbv		26.1		
1x1 Northeastern US	Mean	ppbv	49.6	84.9	81.1	85.1
	Standard Deviation	ppbv	10.2	12.8	16.7	17.3
	Variability	%	21%	15%	21%	20%
	Bias	ppbv		35.3		

817
818
819
820
821
822
823
824

Table 1: Statistical Summary of the CASTNET observations and the three CAM-chem simulations for different spatial averaging regions within the US. Variability is defined as the standard deviation divided by the mean value (in percent). Biases are only included for the present-day CAM-chem simulation compared to the CASTNET data. Similar tables for the other regions in this study are included in the Supplemental Material.